IEEE Access
Multidisciplinary | Rapid Review | Open Access Journal

Received 22 September 2022, accepted 6 October 2022, date of publication 12 October 2022, date of current version 20 October 2022.

Digital Object Identifier 10.1109/ACCESS.2022.3213815

RESEARCH ARTICLE

Research on Object Panoramic 3D Point Cloud Reconstruction System Based on Structure From Motion

XUEJING ZHANG[1,2], JINGYAN LIU[2], BO ZHANG[2], LEI SUN[2], YUHONG ZHOU[2], YUCHAO LI[2], JUN ZHANG[2], HAO ZHANG[2], AND XIAOFEI FAN[1,2]

[1]State Key Laboratory of North China Crop Improvement and Regulation, Hebei Agricultural University, Baoding 071000, China
[2]College of Mechanical and Electrical Engineering, Hebei Agricultural University, Baoding 071000, China

Corresponding author: Xiaofei Fan (hbaufxf@163.com)

This work was supported in part by the National Natural Science Foundation of China under Grant 32072572, in part by the Key Research and Development Program of Hebei Province under Grant 20327403D, in part by the Hebei Talent Support Foundation under Grant E2019100006, in part by the Talent Recruiting Program of Hebei Agricultural University under Grant YJ201847, in part by the Fundamental Research Funds Project of Hebei Agricultural University under Grant KY2021023, and in part by the Special project of talent research introduced by Hebei Agricultural University under Grant YJ2020064.

ABSTRACT 3D reconstruction is the transformation of real objects into mathematical models. By using 3D models, we can observe the shape and measure the parameters, and help us to analyze the properties of objects. For the problems of incompleteness and inefficiency in the reconstruction of object 3D point clouds, a fast and automated system for panoramic 3D point cloud reconstruction of objects was proposed. First, we designed an automatic platform, which could acquire RGB image sequences of objects in two directions. Then we adopted the Structure From Motion (SFM) algorithm to generate point clouds. For the problem of different scales of point clouds, we obtained the scaling by calculating the length ratio of the axes of the oriented bounding box, and scaled the point clouds to a uniform scale. In addition, markers were placed around the object and used to acquire the rotation matrix of the object point cloud in two directions. Finally, we verified the point cloud models of different objects generated by the system, and found that the relative error didn't exceed 6.67%. According to the results, the system proposed could reconstruct the panoramic 3D point cloud of the object better and provide a reference for related research.

INDEX TERMS Panoramic 3D reconstruction, structure from motion (SFM), point cloud scaling, point cloud alignment.

I. INTRODUCTION

With the development of science and technology, the use of computers to construct 3D models of real scenes has become an essential part of many fields before starting in-depth studies [1], [2], [3]. For example, in the agricultural production, 3D reconstruction of crops and animals is adopted to obtain phenotypic parameters [4], [5]. In medical treatment, 3D CT images are used to determine medical conditions [6], [7]. Moreover, in heritage conservation [8], [9], 3D restoration of heritage is performed. At present, 3D reconstruction techniques are also widely applied in multiple fields, such as game development, industrial design, aerospace, and navigation.

Structure From Motion (SFM) is a 3D reconstruction technique based on the basic principle of multi-view geometry, which has the advantages of self-correction and less constraint from the environment. Only 2D image sequences of objects captured by RGB cameras are needed to obtain 3D point clouds. Therefore, it has been very commonly used in 3D reconstruction [10], [11]. In practice, however, we can only obtain 3D point cloud data of single or multiple views of the object for each measurement, and there is also the problem of shadow occlusion in obtaining the complete 3D point cloud data. Thus, it cannot meet the needs of the industry. How to get the complete panoramic 3D point cloud data of the object

The associate editor coordinating the review of this manuscript and approving it for publication was Md. Moinul Hossain.

is a key problem that should be solved in the field of 3D reconstruction [12], [13].

The key to building a panoramic 3D point cloud of an object is to obtain a full range of point cloud data and to align the point cloud data acquired from multiple views. Prior to point cloud alignment, it is sometimes necessary to scale the point cloud to the same scale, as the point clouds generated from different views differ in scale due to the accuracy of the sensor and the distance from the camera. In terms of point cloud scaling, Ying and Du et al., combined the boundary scale and traditional Iterative Closest Point (ICP) algorithm. Have proposed Scaling Iterative Closest Point (SICP) algorithm, which combines the scale factor with the traditional ICP algorithm for alignment, and determines the scale factor, rotation matrix and translation matrix by the minimum distance sum between the point cloud to be aligned and the model point cloud, but the algorithm does not take into account the inconsistent amount of point cloud data [14], [15]. Sun et al., by inscribing the centre of gravity and the centre of mass of a point cloud, have build a scale factor model based on their correspondence, thus scaling different point cloud models to the same scale before alignment, but this method is only applicable to point cloud models with identical shapes [16]. Zhang et al., have proposed a point cloud alignment method based on adaptive neighbourhood matching that can align point clouds of different scales, but it runs slowly [17]. Moreover, the point cloud alignment is a key technology in 3D reconstruction.

Over the past few years, a lot of research results on multi-view point cloud data alignment have been put forward at home and abroad. For example, (ICP) algorithm proposed by Besl and Mckay [18] in 1992 is a classical point cloud alignment algorithm, and the ICP algorithm and its improvements [19], [20], [21] have also become the most widely used alignment algorithms in the industry. However, the results of such algorithms are dependent on the relative positional relationships of the point cloud data. If the initial values are not chosen properly, the ICP algorithm will directly produce erroneous results. The coarse alignment technique, which provides a better initial value for the ICP algorithm, can effectively solve this problem. Apart from that, some scholars use the labeling method [22], [23] for coarse stitching of point cloud data, and determine the position relationship between different angles by pasting some marked points on the object. However, these marker points may obscure the object to be measured, resulting in the missing of point cloud data at some locations. In addition, some scholars align the point cloud by extracting the surface features of the object, which requires the object to be measured to have more obvious and non-universal features [24], [25]. At the same time, some other scholars utilize a rotary table to obtain point cloud data of objects at different angles, and perform point cloud alignment based on the angular relationship of the rotary table rotation [26], [27]. Nevertheless, the calibration process of the rotary table coordinate system is complicated and prone to cause errors, and the bottom surface information of the object placed on the rotary table cannot be captured.

In order solve the problems of incompleteness and inefficiency in the process of object 3D point cloud reconstruction, a panoramic 2D image acquisition platform had been constructed in this study. The platform could acquire a 360° 2D image of the object. Then, the SFM method was used to process the image and obtain the panoramic 3D point cloud of the object. For the alignment problem of point clouds with different scales in two views, we proposed a method to unify the scales of the point clouds of two views using OBB wraparound boxes. Afterwards, the alignment of the fold markers was adopted to obtain the transformation matrix, and then the transformation matrix was applied to the object point cloud to build a panoramic 3D point cloud model of the object. As shown by the experimental results, the proposed pipeline could better build a panoramic 3D point cloud model of the object, which could provide a reference for observation, phenotype measurement, and other work.

II. SYSTEM DESIGN

A. HARDWARE DESIGN AND DATA COLLECTION

The experimental data were obtained from Hebei Agricultural University, and the experimental site was located at the laboratory of the Industrial Training Building of Hebei Agricultural University, Baoding, Hebei, China. In this study, an automatic 2D image sequence acquisition platform was built to acquire the image sequences of the top and bottom of the object in both directions. The image acquisition platform is shown in Figure 1. During the experiment, we placed the object in the middle of the transparent glass carrier on the platform and set the pulse emission frequency of the turntable controller to 1800 HZ. Apart from that, two rotating arms drove the upper and lower RGB cameras to capture 2D images of the object at 2S intervals, each camera rotated 360°, and a total of 50-60 images had been captured. The RGB camera (Model: FS-3200D-10GE, JAI) was a 2-CMOS multi-spectral prism camera. It employed two prism-mounted 3.2 megapixel CMOS imagers which were aligned with a common optical path for image alignment regardless of motion or viewing angle. In order to obtain the point cloud data with clear view and high quality, we had made several attempts. Finally, we adjusted the rotating arm to 45° from the horizontal direction, with the camera being 0.5m away from the object, took a lens with a 25 mm focal length for shooting, and minimized the interference from the surrounding environment.

After acquisition of the image sequences, we manually selected several points of the object, measured the distance between them with a straightedge, and took them as the true values. Beyond that, the same positions of the point cloud model reconstructed by the system were measured, and the two were compared to verify the accuracy of the 3D reconstruction.

In order to align the point cloud model of the object obtained in the upper and lower directions, we took an

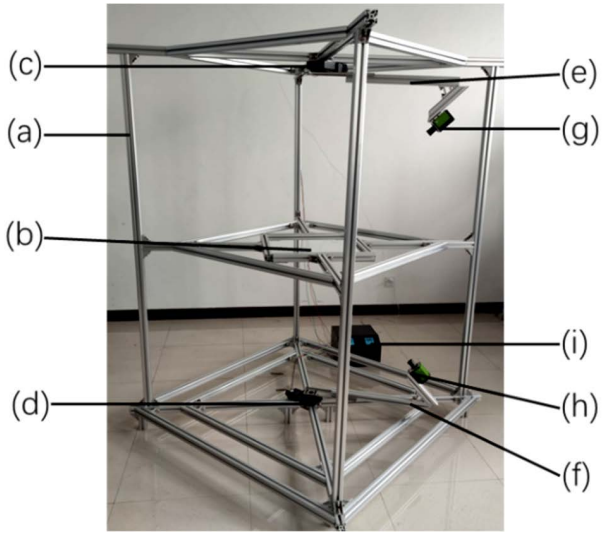

FIGURE 1. (a) Main frame (b) Transparent glass carrier (c) First speed-controlled turntable (d) Second speed-controlled turntable (e) First rotating arm (f) Second rotating arm (g) First RGB camera (h) Second RGB camera (i) Touch interaction interface.

image of the object with markers around the object, which were 6cm x 3cm lines drawn with a signature pen. In addition, the markers were used to obtain the dimensional relationship between the object point cloud and the real world.

In this study, a small body kettle, hammer, cardboard box, power supply, book, multimeter, box ruler, and potted plant were used to perform 3D reconstruction experiments so as to get the final object point cloud model. Meanwhile, the data acquisition, processing and analysis were based on Intel i5- 9300H@2.40GHz Processor, 8GB memory, Windows10 system, camera driver EBUS player for Jai, compiler Microsoft Visual Studio 2017, PCL point cloud Library (1.8.1), open-source software cloudcompare and 3D reconstruction software Agisoft Metashape Professional.

B. SYSTEM WORKING PROCESS

In this system, we first built a platform for the automatic acquisition of panoramic 2D image sequences, and then combined the SFM algorithm as well as some point cloud processing methods which could reconstruct a panoramic 3D point cloud model of an object quickly and automatically. Finally, we measured the object point cloud model and compared it with the real value of the object to verify the accuracy of the 3D reconstruction.

Specifically, we first marked around the target object, acquired 2D image sequences of the object from the top and bottom directions, and used the SFM method to obtain point clouds in each of the two directions. In addition, we segmented the acquired point clouds in two directions to get the target object point cloud and the marker point cloud, respectively. The upper object point cloud and the marker point cloud were taken as a part, the lower object point cloud and the marker point cloud were taken as a part, the scaling was obtained by calculating the axial length of the enclosing box, and then the two parts were scaled to a uniform scale. After scaling the upper point cloud to the same scale as the lower point cloud, we split out the markers in both directions, aligned the marker point clouds to get the transformation matrix, and then applied the transformation matrix to the object point clouds to complete the point cloud alignment of the object in both directions. Lastly, we measured the parameters of the object's 3D point cloud model to verify the accuracy of the 3D reconstruction. Figure 2 shows the system working process.

1) OBJECT 3D POINT CLOUD ACQUISITION

The three-dimensional reconstruction technology based on the images is a technology for restoring 2D images to 3D models [28]. SFM is one of the 3D reconstruction methods, of which the principle is to apply a matching algorithm to an acquired sequence of multi-view images in order to obtain the correspondence of the same pixel points of the image and to use the matching constraint relationship in combination with the triangulation principle to obtain the 3D coordinates of the spatial points and then reconstruct a 3D model of the object [29]. The reconstruction process mainly contains the key steps such as feature point extraction and matching, sparse point cloud reconstruction and dense point cloud reconstruction. Generally speaking, the SFM method has the advantage of being self-correcting and less constrained by the environment. Therefore, we obtain a 3D point-cloud model of the object by using SFM method.

It is inevitable that noise appeared in the target point cloud data due to camera accuracy and external environment, and these point clouds could adversely affect the subsequent point cloud alignment and parameter measurements. Besides, we used a filter based on point cloud neighborhood distance to remove outliers [30].

We manually set the value of the neighborhood and the number of points in the neighborhood to remove the outlier noise. Taking the kettle as an example, Figure 3 shows the process of reconstructing the object image sequence into a point cloud.

At present, the popular 3D reconstruction software using the principle of SFM algorithm includes openMVG, Colmap, VisualSFM and Bundler, etc. In this study, Agisoft Metashape (version 1.8, St. Petersburg, Russia) software was used to obtain the 3D point cloud of the object. After acquisition of the image sequences, we imported the acquired image sequences in the upper and lower directions into Agisoft Metashape software, performed the image alignment step first, and then generated a dense point cloud. For image alignment, we set the calculation accuracy to a high level and the limits for both key points and connection points to 60,000. When generating dense images, we set the generated point cloud quality to a high level, acquired the point cloud color corresponding to the image sequence, and set the filter to a light level so as to reduce the possibility of filtering out important features.

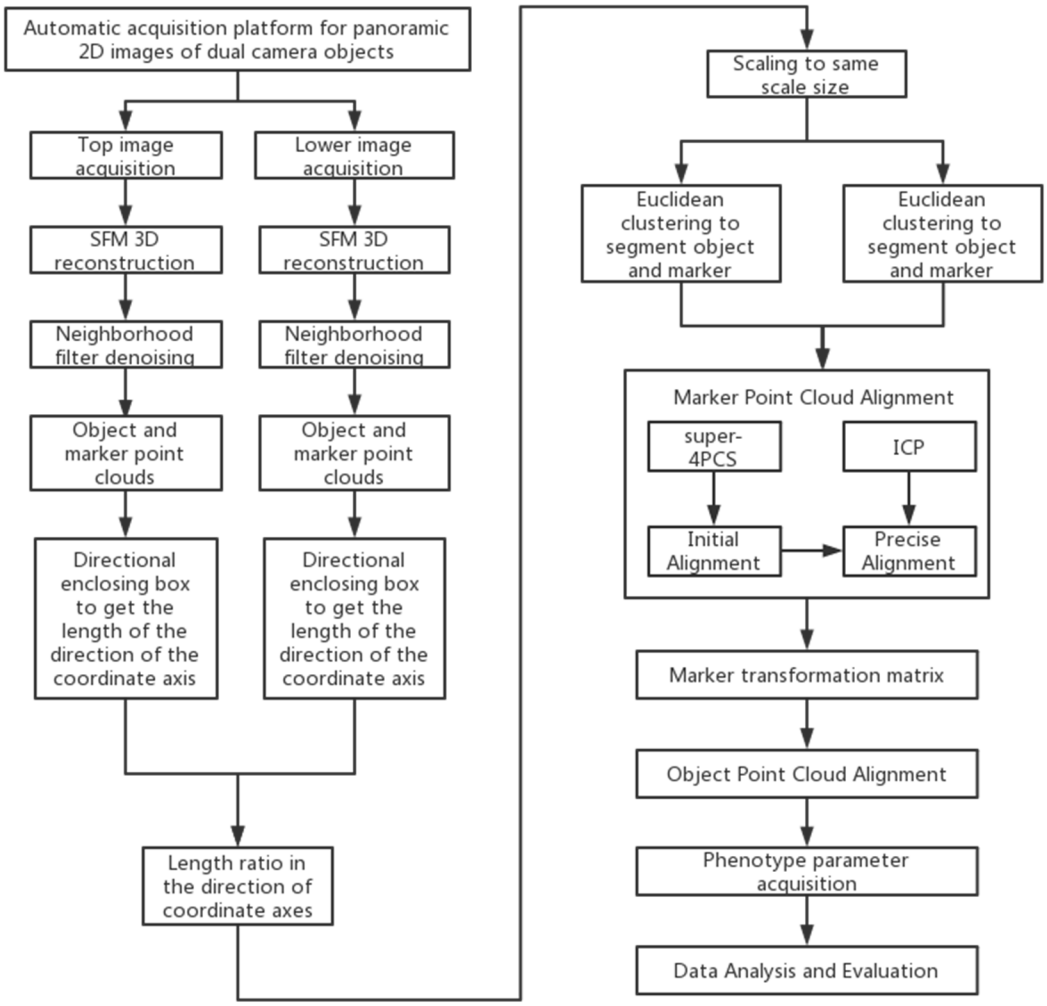

FIGURE 2. System working process.

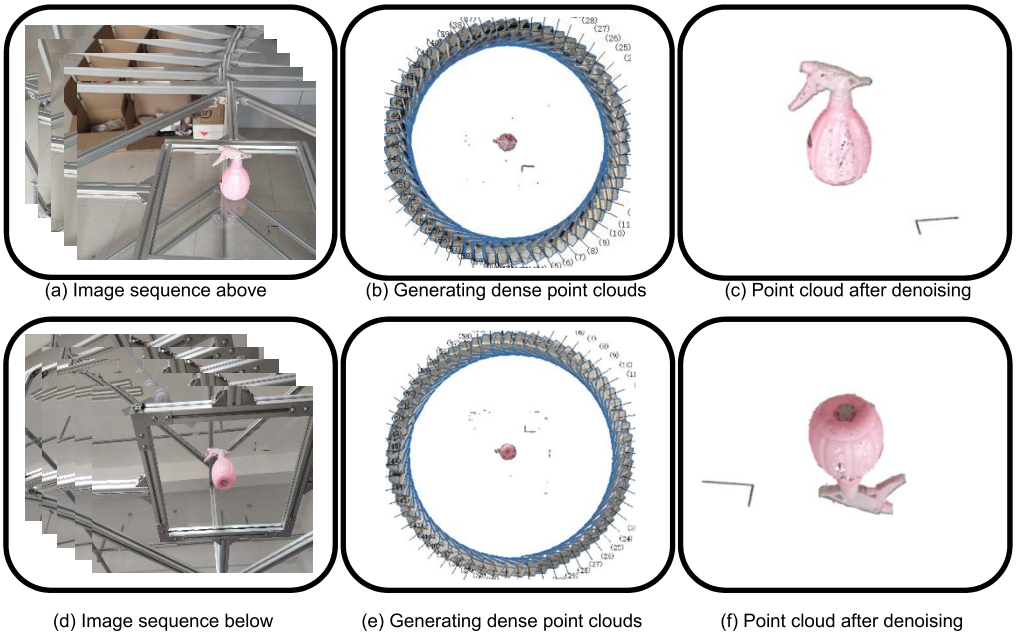

FIGURE 3. Point cloud generation process.

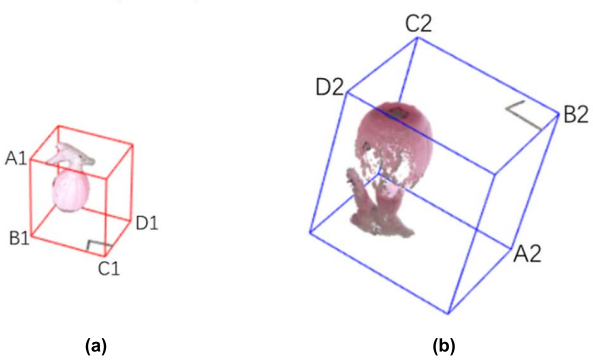

FIGURE 4. Point cloud oriented bounding box generation process. a. oriented bounding box of point cloud P, b. oriented bounding box of point cloud Q.

2) POINT CLOUD SCALE SCALING

Due to the lens accuracy, shooting distance and mechanical vibration of the two cameras, the obtained target point cloud models have the scale inconsistency. If we align them directly, it will lead to large errors. Thus, we first scaled them. The target point cloud and the marker point cloud acquired from above by the camera as a whole are called point cloud P ={P_i |i = 1, . . . , N}. Likewise, the point cloud below is called Q ={Q_i |i = 1, . . . , N}, where N denotes the number of points. In order to unify the scale of point cloud P with point cloud Q, we used Principal Component Analysis (PCA) to construct an oriented bounding box of the point cloud [31], as shown in Figure 4. From this, we derived the lengths of the point cloud in the three axis directions, and took the ratio of the lengths in the X-axis direction as the scaling ratio to scale the point cloud P to the same size as the point cloud Q. The specific procedure is as follows: First we calculated the center of mass m of the point cloud P:

$$m = \frac{1}{N}\sum_{i=1}^{N} P_i \tag{1}$$

Then, we constructed the covariance matrix C

$$C = \frac{1}{N}\sum_{i=1}^{N} (P_i - m)\,(P_i - m)^T \tag{2}$$

We calculated the eigenvalues of the matrix C. The eigenvalues correspond to the eigenvectors $\varepsilon 1$, $\varepsilon 2$, $\varepsilon 3$. Furthermore, these three eigenvectors were taken as the three main directions of the point cloud enclosing the box, respectively. We denoted the matrix A = [$\varepsilon 1$, $\varepsilon 2$, $\varepsilon 3$]. Let

$$\hat{P} = AP \tag{3}$$

Since the three eigenvectors are orthogonal to each other and have modulus 1, we used the eigenvectors as the coordinate axes to establish a new coordinate system, and $\hat{P}$ represents the coordinates of P in the new coordinate system. The maximum and minimum values of $\hat{P}$ in the direction of 3 axes are divided into x_{max}, y_{max}, z_{max} and x_{min}, y_{min}, z_{min}, from which we could get the 8 vertices of the point cloud enclosing the box. Then, the lengths of the oriented bounding box of the point cloud P in the direction of the three axes XYZ could be expressed as:

$$\begin{cases} l_{A1B1} = |x_{max} - x_{min}| \\ l_{B1C1} = |y_{max} - y_{min}| \\ l_{C1D1} = |z_{max} - z_{min}| \end{cases} \tag{4}$$

Similarly, the lengths of the point cloud Q with oriented bounding box in the XYZ axes are l_{A2B2}, l_{B2C2}, l_{C2D2}; Indeed, the two RGB cameras of the image acquisition platform rotate 360° to capture a wide range, the acquired point cloud of the object in two directions contains more information, and only local information is missing. Thus, we took the longest edge of the object in the direction of the three coordinate axes to calculate the ratio as the scaling ratio, which is the most accurate. Apart from that, when we calculated the eigenvalues of the point cloud covariance matrix, the eigenvector corresponding to the largest eigenvalue was used as the coordinate axis, and the point cloud projected to this axis is the most dispersed with the largest variance, and these point clouds are the longest side. Since the eigenvectors corresponding to the largest and smallest eigenvalues are X, Y, and Z axes, and the eigenvector corresponding to the largest eigenvalue is X axis, we calculated the ratio of the length of the object point cloud in the X-axis direction as the scaling ratio k. Then, we got

$$k = \frac{l_{A1B1}}{l_{A2B2}} \tag{5}$$

Next, we scaled each point in the point cloud P. The X,Y,Z coordinates of each point were divided by the corresponding scaling ratio K to get the final result. After scaling, the top and bottom point clouds have the same scale size. The calculation formula could be expressed as follows:

$$P_s = \left(\frac{X_{Pi}}{k}, \frac{Y_{Pi}}{k}, \frac{Z_{Pi}}{k}\right) \tag{6}$$

where P_s represents the scaled point cloud of P, and X_{Pi}, Y_{Pi}, Z_{Pi} represents the x, y, z coordinates of each point in the point cloud P, respectively.

3) POINT CLOUD ALIGNMENT

Due Point cloud alignment is the conversion of multiple local point clouds acquired from different angles into a unified world coordinate system. In general, it consists of two processes: coarse alignment and exact alignment. Coarse alignment provides better positions and initial values for exact alignment, and exact alignment tends to use the ICP algorithm [32]. After removing the noise and scaling the point cloud model, we aligned the point clouds of the object from the top and bottom views to create a panoramic 3D point cloud model of the object. For different objects, the object point clouds obtained from two directions are generally different. If we directly align the object point clouds, the alignment results will be inaccurate or even fail due to the lack of object point cloud features in both directions. In this paper,

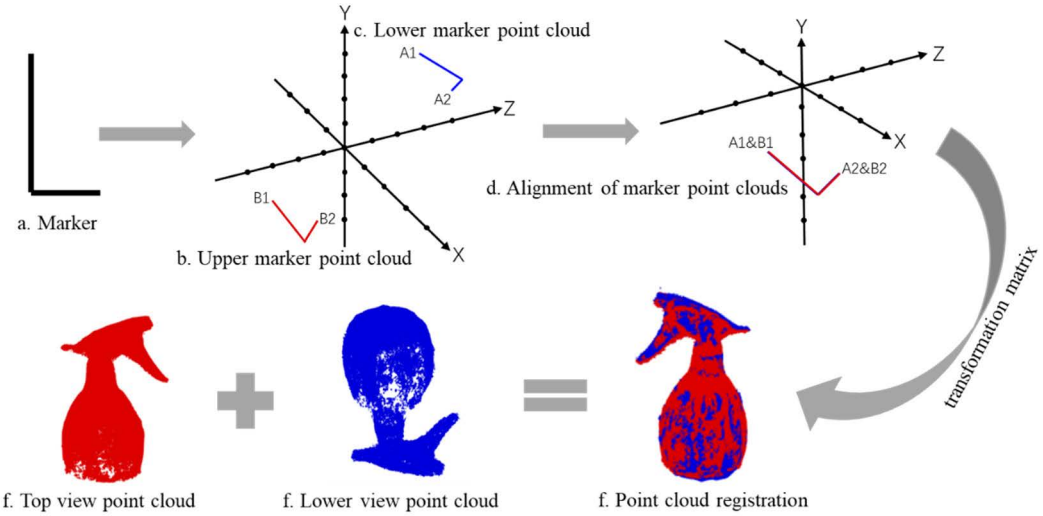

FIGURE 5. Process of point cloud alignment. The marker point clouds are obtained from both the top and bottom views and aligned. After obtaining the transformation matrix, we use this transformation matrix for the alignment of the water bottle.

we drew a line next to the target object as a marker while capturing the image, and then reconstructed it together with the target object. Since the marker is drawn on a transparent glass carrier, and the marker point clouds acquired in both directions completely overlap and align well, we first aligned the marker point clouds. The theory of the classical 4 point Congruent Sets (4PCS) algorithm is based on the affine invariance of coplanar four-point pairs, which reduces the search complexity to zero by using a wide-field basis [33], while the super-4PCS algorithm is an improved version of 4PCS that enables fast extraction of point pairs by the rasterization of the meshing in the target point-cloud, avoiding a global search of the point-cloud data. It uses angular constraints to reduce the generation of invalid point pairs, improving the efficiency and accuracy of the overall point-cloud alignment [34]. Therefore, we have selected the super-4PCS algorithm for the coarse alignment of the markers, followed by the classical ICP algorithm for the exact alignment.

Once the marker point clouds are successfully aligned, the transformation matrix is applied to the object point clouds. Since the relative positions of objects and markers are constant, we also completed the alignment of the object point clouds. Taking a water bottle as an example, Figure 5 displays the point cloud alignment process. In order to better show the effect of point cloud alignment, we rendered the point clouds collected above in red and the point clouds collected below in blue.

C. STATISTICAL ANALYSIS

1) POINT CLOUD SIZE TRANSFORMATION

In order to obtain the real dimensions of the 3D point cloud model, we drew dash markers next to the object during the image sequence of the target object. Apart from that, the markers were used not only for point cloud alignment to obtain the transformation matrix, but also for measuring the true size of the reconstructed point cloud model. In addition, we performed 3D point cloud reconstruction of objects and markers, and then got a conversion ratio of the point cloud length to the real-world length by measuring the distance of the markers. The calculation formula could be expressed as follows:

$$f = \frac{L_{real}}{L_{reconstructed}} \tag{7}$$

where L_{real} represents the real length of the marker, $L_{reconstructed}$ represents the reconstructed model length of the marker, and f represents the conversion ratio.

After calculating the scale factor f, we could obtain the actual size of the reconstructed object in the real world by scale conversion.

2) OBJECT PARAMETER MEASUREMENT

In this paper, we manually selected several points of the object and measured their distances with a straightedge. For each object, we chose two sets of data and compared them with the system reconstruction results to verify the accuracy of the object 3D point cloud reconstruction. When we manually selected points for measurement of objects and object point cloud models, we must ensure the same orientation to reduce errors. To be specific, we selected the following locations of the objects and measured the distances:

(1) the two endpoints of the kettle's choice of grip;
(2) the diameter of the kettle's base;
(3) the length of the hammer;
(4) the diameter of the hammer;
(5) the length of the carton;
(6) the width of the carton;
(7) the length of power;
(8) the height of power;
(9) the length of the book;
(10) the height of the book;

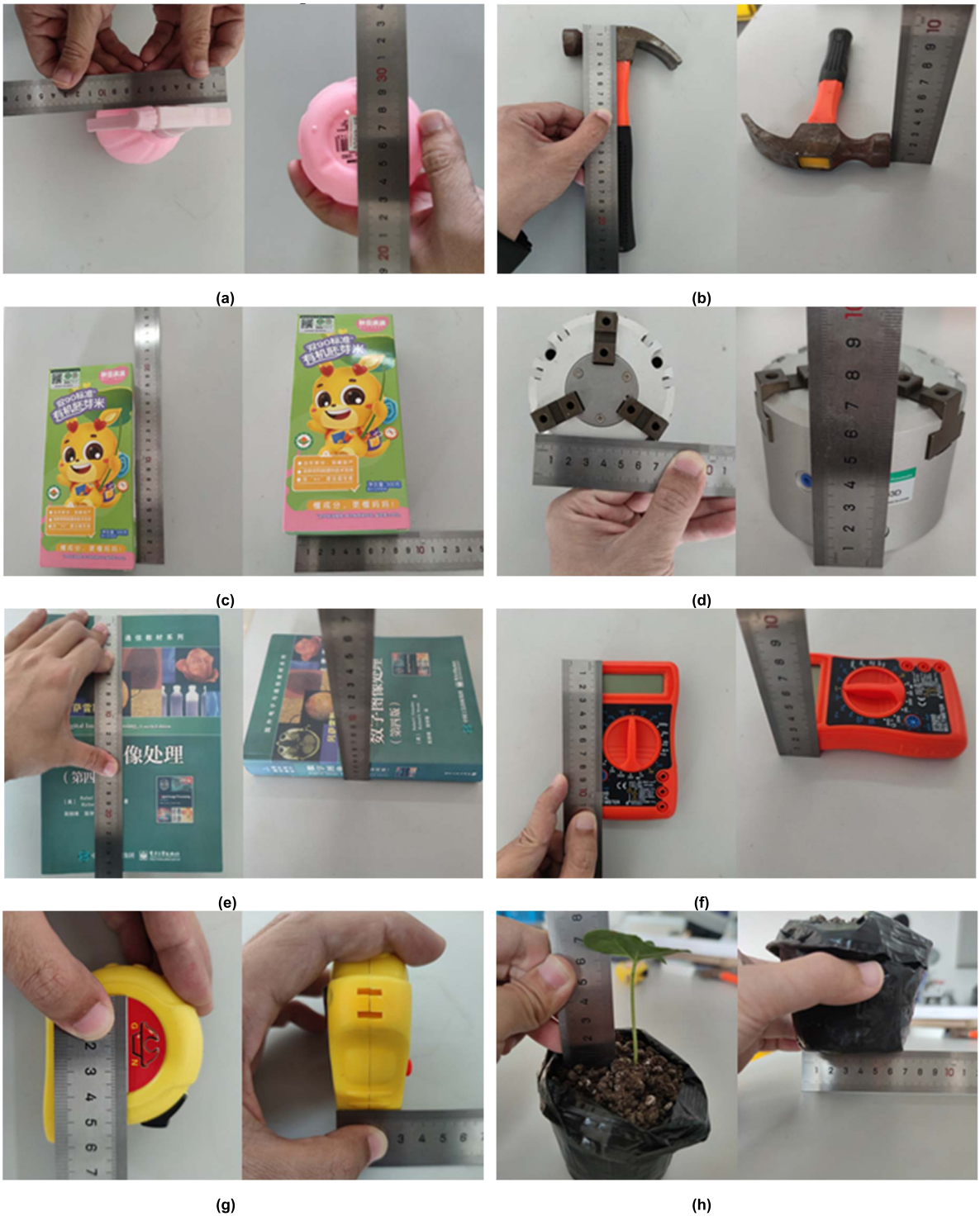

FIGURE 6. Object parameter measurement. (a) measurement of kettle, (b) measurement of hammer, (c) measurement of carton, (d) measurement of power, (e) measurement of book, (f) measurement of multimeter, (g) measurement of box ruler, (h) measurement of flower pot.

(11) the top of the multimeter to the label length;
(12) the height of the multimeter;
(13) the red line on the label of the box ruler;
(14) the thickness of the box ruler;
(15) the stem length of the eggplant seedlings;
(16) the diameter of the base of the flower pot.

In this paper, we also tried to use the minimum wraparound box method to obtain the object point cloud parameters. However, for objects of different shapes, the enclosing box we obtained sometimes deviates from the orientation when the

(a) Initial state (b) The result after scaling

FIGURE 7. Scaling experiment with a water bottle as an example.

real object is measured manually, which leads to the generation of errors. Figure 6 presents the parametric measurement of the object.

III. RESULT

A. POINT CLOUD SCALING RESULTS

Given that the point clouds obtained from the top and bottom directions had different scales, we took the kettle as an example and scaled the point cloud obtained from the top of the kettle. After scaling, the scale was the same as the point cloud below. At this time, the scaling $k = 0.258$, indicating that the scale of the point cloud above is smaller than the scale of the point cloud below. Figure 7 shows the scaling experiment with a water bottle as an example.

B. POINT CLOUD ALIGNMENT RESULTS

For objects with general 3D structure, if 3D reconstruction is performed just in only one direction, the obtained results will be incomplete, which will lead to the loss of local information and inaccurate measurement of phenotypic parameters. In this paper, we used eight different objects for our experiments and obtained the final panoramic 3D point cloud model. The results are shown in Figure 8. In order to better show the effect of point cloud alignment, we intercepted different views of the point cloud model of the object. It can be seen that if only the point cloud of the object is collected in one direction, it will lead to partial loss of information. Besides, the point cloud of the kettle collected from above is without a base. After the alignment of point cloud, the point cloud of the kettle collected from below completes the missing base. In addition, the point cloud of the potted plant from the top view is also without a base, and the point cloud from below completes it. For the other objects, the point clouds of the top and bottom views each occupy nearly one-half of the objects and are combined to form the final point cloud model.

C. OBJECT DATA MEASUREMENT RESULTS

In this paper, we took 2D images of 8 objects and measured the dimensions of the objects at several selected points simultaneously. Then, the proposed pipeline was used to obtain the final 3D point cloud model of the object. Based on the location of the points, we measured the point cloud model of the object for the selected points at the same location to get the values. Then, the point cloud model measurements were converted to the real-world values based on the transformation scale obtained from the markers. The accuracy of the generated 3D point cloud model of the object was verified by comparing it with the real values of the object. The results are shown in Table 1. It can be observed that the relative errors are all controlled within a small range and there is no major drift. According to the results, the measured values of the object point cloud model have a good agreement with the real values. Meanwhile, the object 3D point cloud reconstruction has high accuracy and good visual effect.

TABLE 1. Results of measurements.

Number	True Value(cm)	Measured value(cm)	Absolute error (cm)	Relative Error (%)
1	11.4	11.5	0.1	0.88
2	5.4	5.2	0.2	3.70
3	23.4	22.2	1.2	5.13
4	2.7	2.6	0.1	3.70
5	18.0	18.7	0.7	3.89
6	8.3	8.5	0.2	2.41
7	7.0	7.2	0.2	2.86
8	6.0	6.1	0.1	1.67
9	26.0	26.4	0.4	1.54
10	2.9	3.0	0.1	3.45
11	11.3	11.0	0.3	2.65
12	2.6	2.6	0.0	0.00
13	3.8	3.6	0.2	5.26
14	3.0	3.2	0.2	6.67
15	6.0	6.3	0.3	5.00
16	6.8	7	0.2	2.94

IV. DISCUSSION

With the continuous development of 3D reconstruction technology, significant progress has been made in the study of 3D reconstruction of objects based on various sensors [35]. the traditional methods of 3D reconstruction of objects are destructive, time-consuming, inefficient and costly, so the focus of current research has been on non-destructive, fast, automatic and low-cost 3D reconstruction of objects. At present, the most widely used 3D reconstruction technology contain image-based 3D reconstruction, LiDAR-based 3D reconstruction and RGB-D depth camera-based 3D reconstruction. The developing LIDAR provides an effective tool for 3D reconstruction, such as a 3D laser scanner can acquire a 3D model of the surface of a target object, but requires the user to manually rotate the scanner or the object, which is less efficient and more subjective [36]. LIDAR has improved 3D plant modelling at different spatial and temporal scales in agriculture, increasing the accuracy of extracting plant phenotype data [37], while LIDAR can also be used for autonomous driving of vehicles [38]. However, the difficult point with LiDAR is to achieve high speed data acquisition through hardware and to use algorithms for real time

FIGURE 8. Different views of the object point cloud after alignment.

processing to obtain high accuracy raw point-cloud data. The advent of RGB-D cameras has provided a new solution for the 3D reconstruction of objects [39], but RGB-D cameras have some limitations due to its structure and working principle, such as the need to calibrate the cameras before using. In addition, such cameras have the disadvantage of high power consumption, low resolution and high cost.

In order to build a 3D model that could fully represent the object, we should choose the appropriate 3D scanning technology to model the object in all aspects. If we capture only one side of the object, the shape information may be lost and the 3D model reconstruction may also be incomplete or inaccurate. We use an easy-to-use image-based 3D reconstruction method in this paper, of which, the inexpensive RGB cameras are integrated into a self-built automatic image acquisition platform, thus providing an effective panoramic 3D reconstruction solution for small to medium-sized objects. This plan is made up of hardware devices and algorithms, of which the hardware part of the image acquisition platform is the result of innovative research. By installing a transparent glass pane objective table in the middle of the platform body and installing the object on the objective table, we have captured the upper and lower directions of the object by using two RGB cameras in order to obtain a panoramic image sequence, which generates a 3D point cloud in turn, achieving the goal of automatically capturing the information on the surface of the object. Due to the different shooting distances from the two cameras to the object, platform vibrations and errors such as lens focal length, the 3D point cloud models generated in the two directions have different scale sizes. Therefore, we have proposed a new scaling method based on the construction of point-cloud oriented bounding box, which scales two point-clouds of different scales to the same size before aligning them, avoiding the interference of other factors when scaling and aligning work are carried out simultaneously. The point-cloud data quantity collected in the paper is generally different, so this method is suitable for scaling point-clouds with different amounts of data. In addition, when we capture images of both sides of an object, both cameras always capture the object at the position with the greatest length, regardless of whether the object is placed horizontally or vertically, and we construct a point-cloud oriented bounding

box and obtain the maximum edge length, taking the ratio of the maximum edge length as the scaling ratio, so that the point-cloud can be scaled successfully, even if there is missing local information and the point-cloud shape is not exactly the same, it can be scaled successfully. Due to we measured the ratio of the corresponding edge lengths rather than scaling them according to the point cloud features, the computational effort is reduced. This scaling method is applicable to the 3D reconstruction solution proposed in this paper, and to other point-cloud models acquired by large wide-angle sensors at different scales. Notably, for the marker point cloud to be aligned, we needed to scale the object point cloud together as a whole and then split it out for alignment. If we scale the marker point cloud separately and then align it, in most cases, it is not guaranteed to be scaled the same as the target object point cloud, which will lead to large errors.

The conventional point-cloud alignment methods contain the feature alignment, camera calibration and reference-based methods [40], [41], [42]. The feature alignment method is suitable for the case where the surface features of the object are obvious, provided that the point-cloud has no obvious features or the surface is missing, the alignment shall not be successful. The camera calibration method is to calibrate the sensor in shooting, to obtain information on the position parameters between sensors and to use the position information for alignment, the disadvantage is that the calibration work is tedious and once the shooting position has changed, it has to be recalibrated. During the shooting, we have placed the characteristic markers next to the object, and obtained the rotation matrix by aligning the marker while photographing. The advantage of this is that the object can be successfully aligned regardless of whether the point-cloud features are visible or missing, and the tedious work of calibrating the camera is eliminated. In addition, the 6cm x 3cm fold was selected as the marker, because the marker cannot be symmetrical. If a circle, rectangle, or square is chosen as the marker, the position may be rotated by 90° or 180° when matched. Thus, the fold is chosen as the marker. In addition, it is essential to obtain the dimensions of the markers so as to convert the point cloud model dimensions to the real-world dimensional scale. The panoramic 3D reconstruction scheme in this paper has the advantage of being fast, automatic and low-cost compared to current panoramic 3D reconstruction methods such as the handheld 3D scanner method and turntable calibration method, which reduce subjectivity, inefficiency and partial information loss. After 3D reconstruction of the target object, we can establish a mathematical model suitable for computer representation and processing, so that we can process, manipulate and analyze its properties in a computer environment.

We measured the dimensions of the final obtained 3D point cloud model of the object and compared them with the real values with high accuracy. According to the data results, the system is reliable, less costly, and more flexible in application scenarios than other techniques such as LIDAR and laser scanning to obtain 3D point cloud models of objects through 3D reconstruction [43], [44]. However, it also has some limitations. In general, the traditional ICP algorithm is suitable for aligning point clouds with close spatial distance and obvious features. When the two-point clouds have different spatial locations and obscure features, the ICP algorithm can easily fall into local optimal solutions. Therefore, we first used coarse alignment to make the two marker point clouds get a better relative spatial position.

In this study, we had tried various methods for point cloud coarse alignment and finally chose the super-4PCS algorithm, which has faster speed and higher efficiency in comparison to other methods. After completion of the coarse alignment, the point cloud has a better spatial relative position. Then, we used the ICP algorithm for exact alignment, which not only improves the alignment accuracy but also shortens the alignment time. Beyond that, we obtained the transformation matrix by aligning the markers and then applying the transformation matrix to the objects, which thus avoided alignment failure due to insufficient point cloud features of objects with different viewpoints.

For the acquired image sequences, there are up to several dozens of images in the upper and lower directions, respectively. The process of taking these images as input and reconstructing the 3D point cloud occupies most of the system's time. For the hardware device applied in this study, it took 40 - 70 minutes to reconstruct the point cloud of 50 images in one direction by using the software [45], depending on the quality of the images and the accuracy to be achieved. In order to speed up the process of re-constructing point clouds, we could choose better hardware devices or sacrifice the quality of the point cloud model. With the development of computer vision technology, it is hoped that more efficient SFM 3D reconstruction methods will emerge.

V. CONCLUSION

For the problems of incompleteness and inefficiency in the reconstruction of target point clouds by traditional methods, this paper proposed a fast and automated 3D whole point cloud reconstruction system. Firstly, we built a 2D image sequence automatic acquisition platform, which could acquire the upper and lower directions of the object, and combine the SFM algorithm to generate 3D point cloud models of the object in two directions. Furthermore, we obtained the scaling by calculating the length of the axes of the oriented bounding box, and then scaled the point clouds to a uniform scale. Then, we segmented the target and the marker and aligned the marker point cloud. After getting the transformation matrix, we applied it to the object point cloud and finally got the 3D point cloud model of the object.

By using the fixed-point measurement method, we acquired the target point cloud model values and compared the results with the actual values, which showed a good agreement. At the same time, the phenotype size after object 3D reconstruction alignment had high accuracy and good visual effect. As shown by the results, the panoramic 3D reconstruction system designed in this paper could better reconstruct the panoramic 3D point cloud model of the object and provide a

reference for observation and parameter measurement. However, due to the limitation of hardware size, this system could only perform panoramic 3D point cloud reconstruction for some small and medium-sized objects. In the future research, we will continue to optimize this system, and explore faster and more accurate point cloud alignment methods to increase the efficiency.

ACKNOWLEDGMENT

(Xuejing Zhang and Bo Zhang are co-first authors.)

REFERENCES

[1] Z. Kang, J. Yang, Z. Yang, and S. Cheng, "A review of techniques for 3D reconstruction of indoor environments," *ISPRS Int. J. Geo-Inf.*, vol. 9, no. 5, p. 330, May 2020, doi: 10.3390/ijgi9050330.

[2] A. K. Ingale and U. J. Divya, "Real-time 3D reconstruction techniques applied in dynamic scenes: A systematic literature review," *Comput. Sci. Rev.*, vol. 39, Feb. 2021, Art. no. 100338, doi: 10.1016/j.cosrev.2020.100338.

[3] C. Liu, D. Kong, S. Wang, Z. Wang, J. Li, and B. Yin, "Deep3D reconstruction: Methods, data, and challenges," *Frontiers Inf. Technol. Electron. Eng.*, vol. 22, no. 5, pp. 652–672, May 2021.

[4] S. Shuai, Y. Ling, L. Shihao, Z. Haojie, T. Xuhong, L. Caixing, S. Aidong, and L. Hanxing, "Research on 3D surface reconstruction and body size measurement of pigs based on multi-view RGB-D cameras," *Comput. Electron. Agricult.*, vol. 175, Aug. 2020, Art. no. 105543, doi: 10.1016/j.compag.2020.105543.

[5] X. Ma, B. Wei, H. Guan, and S. Yu, "A method of calculating phenotypic traits for soybean canopies based on three-dimensional point cloud," *Ecological Informat.*, vol. 68, May 2022, Art. no. 101524.

[6] S. Serte and H. Demirel, "Deep learning for diagnosis of COVID-19 using 3D CT scans," *Comput. Biol. Med.*, vol. 132, May 2021, Art. no. 104306, doi: 10.1016/j.compbiomed.2021.104306.

[7] B. Dane, T. O'Donnell, S. Liu, E. Vega, S. Mohammed, V. Singh, A. Kapoor, and A. Megibow, "Radiation dose reduction, improved isocenter accuracy and CT scan time savings with automatic patient positioning by a 3D camera," *Eur. J. Radiol.*, vol. 136, Mar. 2021, Art. no. 109537, doi: 10.1016/j.ejrad.2021.109537.

[8] L. Song, X. Li, Y.-G. Yang, X. Zhu, Q. Guo, and H. Liu, "Structured-light based 3D reconstruction system for cultural relic packaging," *Sensors*, vol. 18, no. 9, p. 2981, Sep. 2018, doi: 10.3390/s18092981.

[9] E. K. Webb, S. Robson, and R. Evans, "Quantifying depth of field and sharpness for image-based 3D reconstruction of heritage objects," *Int. Arch. Photogramm., Remote Sens. Spatial Inf. Sci.*, vol. 43, pp. 911–918, Aug. 2020, doi: 10.5194/isprs-archives-XLIII-B2-2020-911-2020.

[10] S. Yamauchi and K. Suzuki, "Verification of model accuracy and photo shooting efficiency of large-scale SfM for flight path calculation," *J. Robot. Mechatronics*, vol. 33, no. 2, pp. 322–328, Apr. 2021, doi: 10.20965/jrm.2021.p0322.

[11] Y. Yang, Y. Shi, X. Liang, T. Huang, S. Fu, and B. Liu, "Evaluation of structure from motion (SfM) photogrammetry on the measurement of rill and interrill erosion in a typical loess," *Geomorphology*, vol. 385, Jul. 2021, Art. no. 107734, doi: 10.1016/j.geomorph.2021.107734.

[12] J. Huang, J. Stoter, R. Peters, and L. Nan, "City3D: Large-scale building reconstruction from airborne LiDAR point clouds," *Remote Sens.*, vol. 14, p. 2254, May 2022.

[13] X. Zhang, L. Jian, and M. Xu, "Robust 3D point cloud registration based on bidirectional maximum correntropy criterion," *PLoS ONE*, vol. 13, no. 5, May 2018, Art. no. e0197542, doi: 10.1371/journal.pone.0197542.

[14] S. Ying, J. Peng, S. Du, and H. Qiao, "A scale stretch method based on ICP for 3D data registration," *IEEE Trans. Autom. Sci. Eng.*, vol. 6, no. 3, pp. 559–565, Jul. 2009, doi: 10.1109/TASE.2009.2021337.

[15] S. Du, N. Zheng, L. Xiong, S. Ying, and J. Xue, "Scaling iterative closest point algorithm for registration of m–D point sets," *J. Vis. Commun. Image Represent.*, vol. 21, nos. 5–6, pp. 442–452, Jul. 2010, doi: 10.1016/j.jvcir.2010.02.005.

[16] S. F. Sun, Z. Li, K. Xia, Y. Shi, J. Yang, and F. Dong, "Variable scale point cloud registration algorithm," *J. Syst. Simul.*, vol. 30, pp. 2465–2474, Jul. 2018, doi: 10.16182/j.issn1004731x.joss.201807005.

[17] S.-L. Zhang, Y.-Z. Xu, M.-Q. Zhou, G.-H. Geng, and Y.-H. Zhang, "Registration of point clouds based on matching of general adaptive neighborhood," *Chin. J. Comput.*, vol. 42, pp. 2114–2126, Jan. 2019, doi: 10.11897/SP.J.1016.2019.02114.

[18] P. J. Besl and N. D. Mckay, "A method for registration of 3-D shapes," *IEEE Trans. Pattern Anal. Mach. Intell.*, vol. 14, no. 2, pp. 239–256, Feb. 1992, doi: 10.1109/34.121791.

[19] Y. Ren, L. Wang, K. Lin, H. Ma, and M. Ma, "Improved iterative closest contour point matching navigation algorithm based on geomagnetic vector," *Electronics*, vol. 11, no. 5, p. 796, Mar. 2022.

[20] J. Yi, S. Zhang, Y. Cao, E. Zhang, and H. Sun, "Rigid shape registration based on extended Hamiltonian learning," *Entropy*, vol. 22, no. 5, p. 539, May 2020, doi: 10.3390/e22050539.

[21] Y. Xian, J. Xiao, and Y. Wang, "A fast registration algorithm of rock point cloud based on spherical projection and feature extraction," *Frontiers Comput. Sci.*, vol. 13, pp. 170–182, Feb. 2019.

[22] C. S. Chua and R. Jarvis, "Point signatures: A new representation for 3D object recognition," *Int. J. Comput. Vis.*, vol. 25, no. 1, pp. 63–85, Oct. 1997, doi: 10.1023/A:1007981719186.

[23] Y. Huang and D. M. Umulis, "A point matching algorithm for point set registration," in *Proc. 9th Int. Congr. Image Signal Process., Biomed. Eng. Informat. (CISP-BMEI)*, Datong, China, Oct. 2016, pp. 756–760.

[24] N. A. Sheik, G. Deruyter, and P. Veelaert, "Plane-based robust registration of a building scan with its BIM," *Remote Sens.*, vol. 14, no. 9, p. 1979, Apr. 2022, doi: 10.3390/rs14091979.

[25] W. Tao, X. Hua, Z. Chen, and P. Tian, "Fast and automatic registration of terrestrial point clouds using 2D line features," *Remote Sens.*, vol. 12, no. 8, p. 1283, Apr. 2020.

[26] Y. Ye and Z. Song, "An accurate 3D point cloud registration approach for the turntable-based 3D scanning system," in *Proc. IEEE Int. Conf. Inf. Autom.*, Lijiang, China, Aug. 2015, pp. 982–986.

[27] S. Chaivivatrakul, L. Tang, M. N. Dailey, and A. D. Nakarmi, "Automatic morphological trait characterization for corn plants via 3D holographic reconstruction," *Comput. Electron. Agricult.*, vol. 109, pp. 109–123, Nov. 2014.

[28] A. Shapii, S. Pichak, and Z. R. Mahayuddin, "3D Reconstruction technique from 2D sequential human body images in sports: A review," Kansai Univ., Tech. Rep., 2020, pp. 4973–4988, vol. 62.

[29] M. Kholil, I. Ismanto, and M. N. Fu'Ad, "3D reconstruction using structure from motion (SFM) algorithm and multi view stereo (MVS) based on computer vision," in *Proc. IOP Conf. Mater. Sci. Eng.*, vol. 1073, Feb. 2021, Art. no. 012066, doi: 10.1088/1757-899X/1073/1/012066.

[30] Y. Duan, C. Yang, and B. Li, "Low-complexity adaptive radius outlier removal filter based on PCA for LiDAR point cloud denoising," *Appl. Opt.*, vol. 60, pp. 1–7, Jul. 2021, doi: 10.1364/AO.416341.

[31] B. Wang, M. Zhu, Y. Lu, J. Wang, W. Gao, and H. Wei, "Real-time 3D object detection from point cloud through foreground segmentation," *IEEE Access*, vol. 9, pp. 84886–84898, 2021.

[32] J. Han, P. Yin, Y. He, and F. Gu, "Enhanced ICP for the registration of large-scale 3D environment models: An experimental study," *Sensors*, vol. 16, no. 2, p. 228, 2016.

[33] C. Fotsing, N. Nziengam, and C. Bobda, "Large common plansets-4-points congruent sets for point cloud registration," *ISPRS Int. J. Geo-Inf.*, vol. 9, no. 11, p. 647, Oct. 2020, doi: 10.3390/ijgi9110647.

[34] N. J. Mitra, N. Mellado, and D. Aiger, "Super 4PCS fast global pointcloud registration via smart indexing," *Comput. Graph. Forum*, vol. 33, no. 5, pp. 205–215, Aug. 2014.

[35] J. A. Gibbs, M. Pound, A. P. French, D. M. Wells, E. Murchie, and T. Pridmore, "Approaches to three-dimensional reconstruction of plant shoot topology and geometry," *Funct. Plant Biol.*, vol. 44, pp. 62–75, Aug. 2017, doi: 10.1071/FP16167.

[36] Y. Li, C. Xu, K. Liao, and H. Zhao, "Application of handheld 3D laser scanner in quality inspection of industrial components," *Bull. Surv. Mapping*, vol. 8, pp. 102–105, Aug. 2019, doi: 10.13474/j.cnki.11-2246.2019.0261.

[37] S. Jin, X. Sun, F. Wu, Y. Su, Y. Li, S. Song, K. Xu, Q. Ma, F. Baret, D. Jiang, Y. Ding, and Q. Guo, "Lidar sheds new light on plant phenomics for plant breeding and management: Recent advances and future prospects," *ISPRS J. Photogramm. Remote Sens.*, vol. 171, pp. 202–223, Jan. 2021, doi: 10.1016/j.isprsjprs.2020.11.006.

[38] Y. Li, J. Niu, and Z. Ouyang, "Fusion strategy of multi-sensor based object detection for self-driving vehicles," in *Proc. Int. Wireless Commun. Mobile Comput. (IWCMC)*, Limassol, Cyprus, Jun. 2020, pp. 1549–1554.

[39] W. Han, X. Liu, S. Song, and M. Q.-H. Meng, "3D reconstruction of dense model based on the sparse frames using RGBD camera," in *Proc. IEEE Int. Conf. Robot. Biomimetics (ROBIO)*, Dali, China, Dec. 2019, pp. 2726–2731.
[40] B. Wu, J. Ma, G. Chen, and P. An, "Feature interactive representation for point cloud registration," in *Proc. Int. Conf. Comput. Vis. (ICCV)*, Montreal, QC, Canada, Oct. 2021, pp. 5510–5519.
[41] D.-M. Córdova-Esparza, J. R. Terven, H. Jiménez-Hernández, and A.-M. Herrera-Navarro, "A multiple camera calibration and point cloud fusion tool for Kinect V2," *Sci. Comput. Program.*, vol. 143, pp. 1–8, Sep. 2016, doi: 10.1016/j.scico.2016.11.004.
[42] X. Li, P. Wei, J. He, M. Li, M. Zhang, and B. Wen, "Field plant point cloud registration method based on Kinect V3 depth sensors," *Trans. Chin. Soc. Agricult. Eng.*, vol. 37, pp. 45–52, Aug. 2021.
[43] M. Stein, S. Bargoti, and J. Underwood, "Image based mango fruit detection, Localisation and yield estimation using multiple view geometry," *Sensors*, vol. 16, no. 11, p. 1915, 2016.
[44] P. Sodhi, S. Vijayarangan, and D. Wettergreen, "In-field segmentation and identification of plant structures using 3D imaging," in *Proc. IEEE/RSJ Int. Conf. Intell. Robots Syst. (IROS)*, Vancouver, BC, Canada, Sep. 2017, pp. 5180–5187.
[45] M. D. Howland, A. Tamberino, I. Liritzis, and T. E. Levy, "Digital deforestation: Comparing automated approaches to the production of digital terrain models (DTMs) in agisoft metashape," *Quaternary*, vol. 5, no. 1, p. 5, 2022.

XUEJING ZHANG received the bachelor's degree from the College of Modern Science and Technology, Hebei Agricultural University, China, in 2020, where he is currently a Graduate Student with the College of Mechanical and Electrical Engineering.

His research interest includes computer vision.

JINGYAN LIU received the master's degree in agricultural mechanization engineering from Inner Mongolia Agricultural University, China, in 2013, and the Doctorate degree in agricultural electrification and automation from Hebei Agricultural University, China, in 2020.

She is currently a Lecturer at the College of Mechanical and Electrical Engineering, Hebei Agricultural University. Her research interests include computer vision and spectral technology.

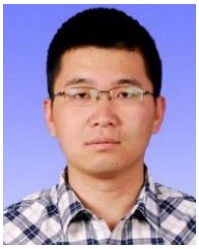

BO ZHANG received the master's degree in agricultural mechanization engineering from Inner Mongolia Agricultural University, China, in 2013.

He is currently a Lecturer at the College of Mechanical and Electrical Engineering, Hebei Agricultural University. His research interest includes intelligent agriculture.

LEI SUN received the master's degree in electrical theory and new technology from North China Electric Power University, China, in 2015, and the Doctorate degree in agricultural electrification and automation from Hebei Agricultural University, China, in 2021.

He is currently a Lecturer at the College of Mechanical and Electrical Engineering, Hebei Agricultural University. His research interests include detection technology and digital agriculture.

YUHONG ZHOU received the master's degree in agricultural electrification and automation from Shenyang Agricultural University, China, in 2008.

She is currently a Lecturer at the College of Mechanical and Electrical Engineering, Hebei Agricultural University. Her research interest includes informatization of local power enterprises.

YUCHAO LI received the bachelor's degree from the Liren College, Yanshan University, China, in 2020. He is currently a Graduate Student with the College of Mechanical and Electrical Engineering, Hebei Agricultural University. His research interest includes computer vision.

JUN ZHANG received the bachelor's degree from the College of Modern Science and Technology, Hebei Agricultural University, China, in 2018, and the master's degree from Hebei Agricultural University, in 2021, where she is currently pursuing the Doctoral degree with the College of Mechanical and Electrical Engineering. Her research interests include computer vision, machine learning, and image processing.

HAO ZHANG received the bachelor's degree from Hebei Agricultural University, China, in 2017, where he is currently a Graduate Student with the College of Mechanical and Electrical Engineering. His research interests include computer vision and image processing.

XIAOFEI FAN received the master's degree in biomedical engineering from Tsinghua University, China, in 2005, and the Doctorate degree in biomedical engineering from the University of Missouri, USA, in 2009.

He is currently a Professor at the College of Mechanical and Electrical Engineering, Hebei Agricultural University. His research interests include computer vision, machine learning, and image processing.